Theor Appl Climatol
DOI 10.1007/s00704-015-1703-8

ORIGINAL PAPER

High-resolution simulation of heatwave events in New York City

P. Ramamurthy[1] · **D. Li**[3] · **E. Bou-Zeid**[2]

Received: 12 March 2015 / Accepted: 2 December 2015

Abstract Heatwave intensity and frequency are predicted to increase in the coming years, and this will bear adverse consequences to the environmental well-being and the socio-economic fabric in urbanized areas. The hazardous combination of increased heat storage and reduced water retention capacities of the land surface make the urban areas warmer than the surrounding rural areas in what is commonly known as the urban heat island (UHI) effect. The primary motives of this study are to quantify the interaction of this city-scale UHI with synoptic-scale heatwave episodes and to analyze the factors that mediate this interaction. A modified version of the Weather Research and Forecasting model (WRF) is utilized to simulate two heatwave episodes in New York City. The land surface scheme in the default WRF model is modified to better represent the surface to atmosphere exchanges over urban areas. Our results indicate that during the heatwave episodes, the daily-averaged UHI in NYC increased by 1.5 K. Furthermore, most of this amplification occurs in the mid-afternoon period when the temperatures peak. Wind direction and urban-rural contrasts in available energy and moisture availability are found to have significant and systematic effects on the UHI, but wind speed plays a secondary role.

✉ P. Ramamurthy
pramamurthy@ccny.cuny.edu

[1] Department of Mechanical Engineering, The City College of New York, New York, NY, USA

[2] Department of Civil and Environmental Engineering, Princeton University, Princeton, NJ, USA

[3] Program of Atmospheric and Oceanic Sciences, Princeton University, Princeton, NJ, USA

1 Introduction

Heatwaves in the near future are predicted to be more frequent, intense, and sustained (Meehl 2004), and they pose a severe threat to human life and property (Melilo et al. 2014). Heatwaves can be defined as extended periods of extreme heat stress, which result in unusually high number of human fatalities (Robinson 2001). The 1995 heatwave episode in the US Midwest resulted in 1000 deaths in the states of Missouri and Illinois (Palecki et al. 2001), and nearly 40,000 people perished in the 2-week long mid-summer heatwave event over Central Europe in 2003 (Martiello and Giacchi 2010). In the last 30 years, heatwaves have claimed more lives in the USA than all other natural disasters combined (Altman 2012). Apart from loss of human life, heatwaves also add severe stress to the infrastructure; power grids are particularly vulnerable to extreme heatwave episodes. As power consumption surges, the probability of blackouts increases. In New York City (NYC) the mortality rate jumped by 25 % as a result of the August 2003 blackout caused by an extreme heat event (Anderson and Bell 2012). Moreover, increased energy consumption during heatwaves leads to higher emissions of greenhouse gases (Hoffert et al. 2002).

Meteorologically, heatwaves are associated with anticyclonic circulation patterns that result in clear sky conditions and subsidence of warm air from the upper atmosphere (Black et al. 2004; Xoplaki et al. 2003). The land-atmosphere coupling is also known to play a major role in the formation and persistence of heatwaves. Fischer et al. (2007) observed that negative soil moisture anomalies from the preceding spring season had a devastating impact on summertime temperatures over Central Europe. The soil moisture anomaly was a result of precipitation deficit, increased the top-of-atmosphere (TOA) radiation due to additional clear sky days, and soil drying due to excess early season evapotranspiration. In urbanized areas, where the natural land cover is replaced by built surfaces, relatively higher daytime and nighttime air temperatures have been observed during

Published online: 15 December 2015

heatwave episodes (Rosenzweig et al. 2005). More worryingly, recent research points to synergistic interactions between heatwaves and urban heat islands (UHIs) that result in temperature anomalies in cities that exceed the sum of the background UHI spatial anomaly (pre-heatwave) and the regional temporal heatwave anomaly (Li and Bou-Zeid 2013). The built materials (asphalt roads, concrete pavements, rooftops, and steel and brick buildings) that predominate the urban landscape have high thermal effusivity, which alters the surface energy balance significantly (Ramamurthy et al. 2014). In addition, the lower albedo of some of these materials like asphalt and the radiative trapping in the complex urban canyons increase the absorption of solar radiation in cities. This enables the dense built-surface cover to efficiently absorb and store heat, resulting in higher surface and near surface air temperatures. Built surfaces also have low moisture retention capacity, thereby increasing the Bowen ratio (ratio of sensible heat flux to latent heat flux). The reduced evapotranspirative cooling makes urban areas in general experience elevated near surface air temperatures compared to the surrounding rural areas and was postulated as being the main contributor to elevated urban temperatures (Li and Bou-Zeid 2013; Li et al. 2015). This difference between urban and nearby rural air temperature is commonly referred to as the Urban Heat Island (UHI) (Oke 1982).

NYC was chosen for this study since it is one of the largest metropolitan regions in terms of urbanized land cover and population. It is also the most densely populated city in the USA (Census Bureau 2011). Moreover, the city and its infrastructure are highly vulnerable to threats posed by heatwaves (Rosenzweig and Solecki 2010; Klein Rosenthal et al. 2014), and it has a long recorded history of UHI observations. As early as 1978, Ellis and Nelson (1978) reported on the high mortality rates in the late summer heatwaves of 1972–1975. Bornstein (1968), observed the influence of UHI on NYC's microclimate. His study found that the intensity of temperature inversion is weaker over the urban core of NYC. Leahey and Friend (1971) also observed a strong mixing layer over NYC indicating stronger surface heat flux. Price (1979) utilized satellite-derived images to identify a 17 °C anomaly in surface temperature between NYC and its surrounding rural area. Lately, Gaffin et al. (2008) used National Weather Service observations to detect a marginal increase in UHI in NYC between 1900 and 2008. This modest warming was responsible for approximately one third of the total warming the city has experienced in the past century. The study also noted that during this period, the average wind speed in NYC reduced by half. Gedzelman et al. (2003) also used weather networks in and around the NYC metropolitan area to study the mesoscale impact on UHI. His analysis found that the average UHI increased from 3 °C in the spring and winter to 4 °C in the summer and autumn. The analysis also highlighted the role played by sea breezes in delaying and displacing the UHI during summer months. In addition to observational analysis, some numerical studies have also been conducted to study heat events in NYC. Meir et al. (2013) simulated two extreme heat events in NYC using the coupled ocean/atmosphere mesoscale predictive system (COAMPS) and highlighted the influence of sea breeze on daytime air temperature in NYC. Rosenzweig et al. (2009) used NCAR's mesoscale model (MM5) to explore pertinent mitigation strategies to moderate UHI impacts in NYC. Apart from these NYC-centered numerical studies, other numerical studies have been conducted over various cities to study the impact of heatwaves in urban areas (Salamanca et al. 2012; Giannaros et al. 2013; Zhang et al. 2009). These studies have collectively shown that numerical tools can be effectively used to improve our understanding of the urban microclimate during extreme heat conditions, and of potential approaches for mitigation.

Our study, centered on NYC, will focus on understanding the interaction between synoptic-scale heatwaves and micro/local-scale UHI. The study will also highlight the current advances in urban numerical weather simulations. This analysis will use the state of the art Weather Research and Forecasting (WRF) model to simulate two heatwave events in July 2006. For this study, a version of the WRF model modified in two major ways to better represent the urban microclimate was used: (1) the basic single-layer urban canopy model was replaced by the Princeton Urban Canyon Model (PUCM) (Wang et al. 2013; Wang et al. 2011) that includes more realistic representation of hydrological processes and subfacet level heterogeneity for urban fluxes, and (2) the dominant approach used to ascertain a single land use category in WRF at every grid point will be substituted with a mosaic approach that solves for the land-atmosphere exchanges from multiple land use categories at every grid cell, and fractionally averages the resulting fluxes (Li et al. 2013). The combination of the two advances in WRF was undertaken specifically for this study, and as such, this is the first evaluation and application of the model that simultaneously exploits these two improvements, both of which are critical for accurate modeling of the urban microclimate. Two heatwave episodes from 2006—one in mid-July (16th–18th) and another in early August (1st–3rd)—are examined. The average daily air temperature during this period increased from 28.8 to 35 °C, and the death rate due to natural causes increased by 8 % (Klein Rosenthal et al. 2014). The analyses will then focus on how the synoptic-scale heatwave episodes interacted with the UHI and also examine the physical mechanisms and the climatological factors that control the diurnal variability of UHI.

2 Modeling framework

The WRF-ARW (ARW stands for advanced research WRF) model (Skamarock et al. 2005) is used for this study. WRF is a non-hydrostatic primitive-equation model that has multiple options for various parameterizations. Figure 1 shows the configuration used for the simulations: three one-way nested domains

with grid horizontal resolutions of 9, 3, and 1 km and 60 vertical levels centered on NYC. The simulations are driven by the North American Regional Reanalysis (NARR) data at 6-h intervals, and the North American Land Use Category Dataset (NLCD) 2006 is used to determine the land use type and the surface properties. The following physical parameterization schemes are used in this study: (i) the rapid radiative transfer model scheme for longwave radiation (Mlawer et al. 1997), (ii) the Dudhia scheme (Dudhia 1989) for shortwave radiation, (iii) the 2D Smagorinsky scheme for horizontal diffusion, (iv) the mosaic Noah land surface model for non-urban surfaces (Li et al. 2013), (v) the Mellor-Yamada-Janjic PBL scheme (Mellor and Yamada 1974) along with the modified Zilitinkevich relationship for thermal roughness length parameterization (Chen and Zhang 2009), and (vi) the PUCM (Wang et al. 2013) along with its calibrated thermal surface properties for urban materials representative of the US Northeast. Cumulus parameterization schemes are not used in the simulations since they are not needed with the high resolutions adopted here. The simulation was started on July 12, 0000 UTC, and a 24-h warm up period was allowed before the data was collected for analysis.

As indicated above, the simulations utilize an urban parameterization scheme. The default single-layer urban canopy model (SL-UCM) inside WRF is replaced by the PUCM. The PUCM, akin to the SL-UCM, is based on the energy exchange framework developed by Kusaka et al. (2001). However, each facet (wall, roof, or road) in the PUCM can be further subdivided into multiple subfacets. For example, the user can specify fractions of white/black/green roofs, brick/concrete walls, and concrete/asphalt/vegetated grounds. The multiple subfacets can be modeled with distinct physical and thermal properties. Another important improvement in PUCM is the adoption of more realistic representations for hydrological processes, including in-canyon vegetated soils and water storage capacity for impervious materials. The PUCM coupled to WRF has been previously tested and produced better results compared to the default UCM (Li et al. 2014; Li and Bou-Zeid 2014) (we should also note that in the latest releases of WRF many of the PUCM enhancements were included in the default SL-UCM and are now available for use in the public release of the code (Yang et al. 2015)).

Apart from replacing the default UCM, the WRF simulations also use a mosaic approach (Li et al. 2013) to compute the surface fluxes as opposed to the dominant category method used in default WRF-ARW model. In the mosaic approach, instead of fixing a single dominant land use category at each grid point as the only category in that grid cell, the fluxes from the most common n number (n can be varied from 1 to 15 and added as an input in the namelist file of WRF) of land use types in that grid cell are solved for and then fractionally summed to compute the aggregate flux into the atmosphere. The mosaic approach is pertinent for urban modeling as the land use type in most urban areas, even at 1 km grid spacing, is highly variable and there might not necessarily be a dominant land type category. In NLCD 2006, urban areas fall under three categories: low intensity (50 % built cover), medium intensity (90 % built cover) and high intensity (95 % built cover). For example, the land use type for a grid cell inside the borough of Manhattan is as follows: 39 % high intensity urban, 22 % medium intensity urban, 20 % low intensity urban, 10 % green cover and 9 % water. In the default approach, WRF would assume all the area of the grid cell consists of high intensity urban. In the mosaic-based approach, WRF will solve for all five land use categories, maintaining the homogeneity of the overlying air in that grid cell, and will fractionally add the computed fluxes. While the default approach is appropriate for regional scale modeling (36 km - 10 km), the mosaic approach is more suited at much finer resolutions focusing on cities where the variability length scale of the surface is sharply reduced. The mosaic approach also improves the representation of fluxes from various land use categories without the need to further increase the model resolution since it models surface parameters such as temperature, fluxes, and soil moisture at the higher resolution of the land use maps, thereby reducing the computational cost.

3 Model evaluation

The WRF-PUCM simulations are evaluated against the Automated Surface Observing System (ASOS) in situ ground observations and the Moderate Resolution Imaging Spectroradiometer (MODIS) satellite data. Figure 2 compares the land surface temperature derived from MODIS to the simulated skin temperature for July 24, 1130 EDT. The model performs well in capturing the daytime surface temperature. The hot spots that occur in regions dominated by commercial and high intensity urban area (Long Island, lower Manhattan and eastern New Jersey) are well replicated by the model (the hot spot in the Bronx seems to be underestimated). The model also captures the cool spots in the northwestern part of the domain, dominated by deciduous vegetation. The gradient in surface temperature, as we transect from the city to the suburban area and in to the rural area, is reproduced well in the simulations. The surface temperature drops from 313 K in downtown NYC to 297 K in the rural area.

The model results are also compared to the ASOS weather station data in NYC. Figures 3 and 4 contrast the simulated and ASOS-measured 2 m air temperatures and relative humidity at the Central Park (Manhattan) and the John F. Kennedy (JFK) airport (Brooklyn) ASOS locations. The model captures the overall trend in both the air temperature and the relative humidity very well (see root mean square errors in the figure). Particularly, during the heatwave episodes, the model follows the observations very closely. This is partially due to heatwave episodes occurring during clear sky days without any clouds or frontal disturbances. The discrepancy between the predicted and observed values increases when the weather system is perturbed by frontal passages or other non-local influences. The root mean

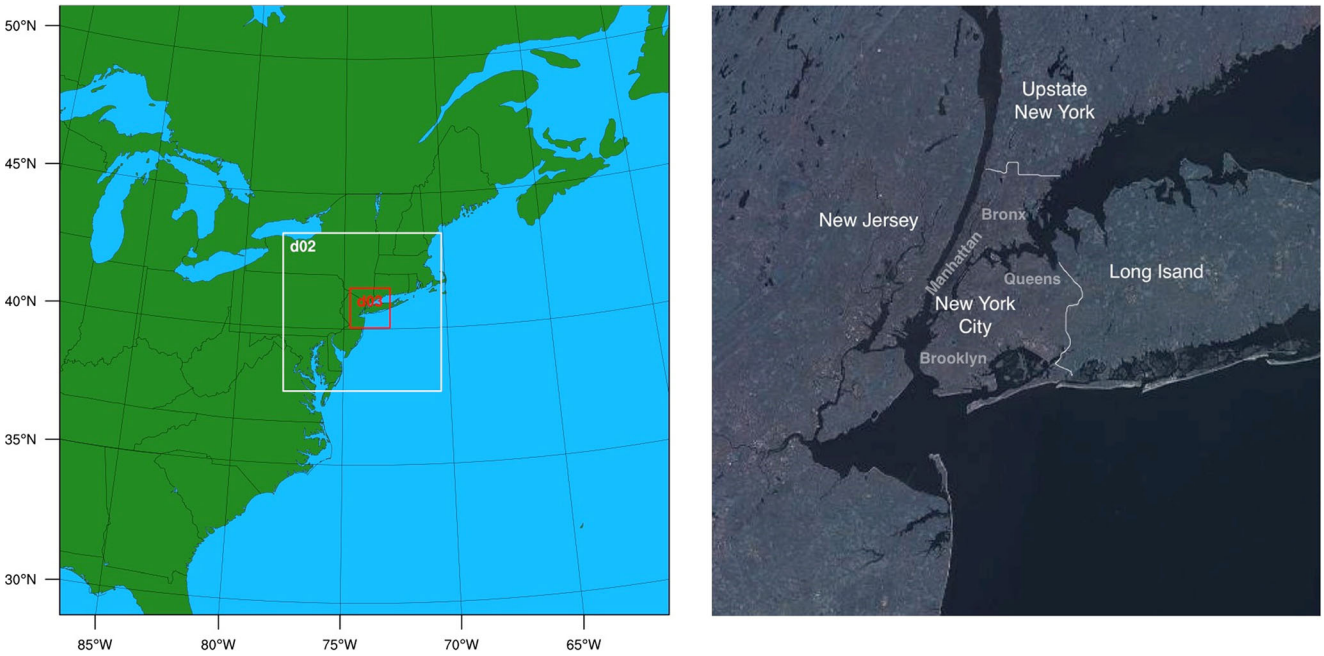

Fig. 1 WRF simulation domain. The domains horizontal resolutions were 9, 3, and 1 km. Domain 3, centered over NYC, had 159 × 159 horizontal grid points and 60 vertical levels. Figure to the right zooms in on domain 3, labeling the landcover over which the simulations were conducted

square errors for the 2-m air temperature and relative humidity for the whole period at the central park station are 2 K and 10 %, respectively, while at the JFK station the root mean square errors are 2 K and 12 %. Given the numerous parameterizations and heterogeneity of urban areas and their complex form, the PUCM-WRF simulations perform very well in reproducing the urban climate and can be used to further our understanding of the dynamics of extreme heat in cities. We would also like to point out that these model evaluation results are much improved compared to previous numerical studies conducted in the NYC area (Rosenzweig et al. 2009; Meir et al. 2013).

4 Results and discussion

Herein we discuss the role played by the 2-heatwave events in amplifying the thermal environment of NYC and also expand

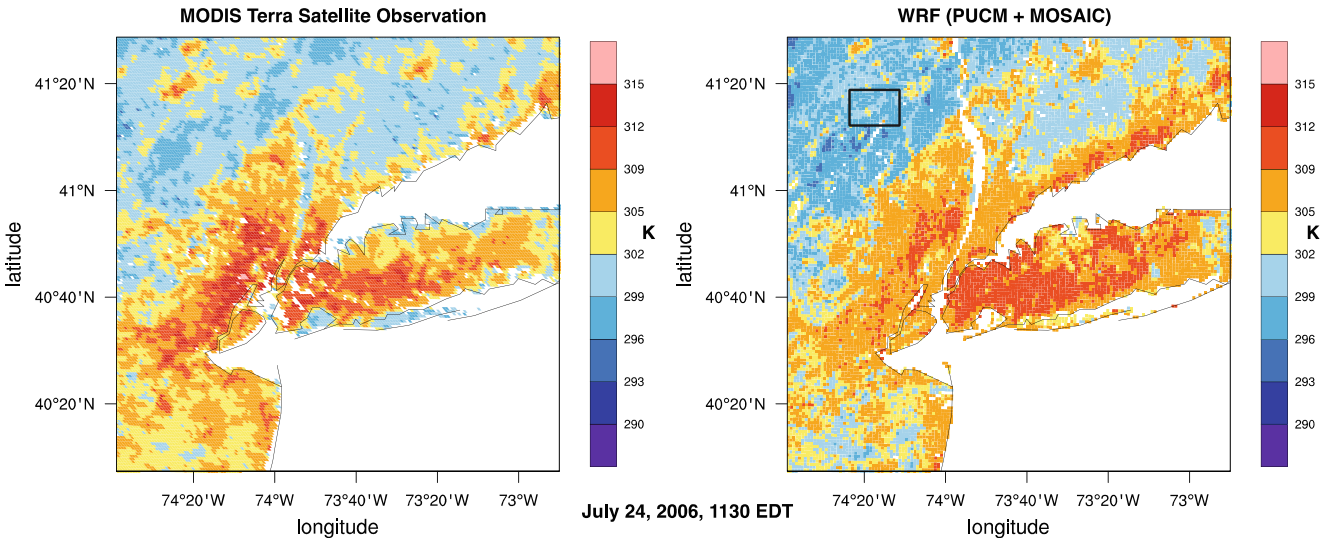

Fig. 2 Comparing MODIS satellite observation to WRF simulation (1 km resolution). The black box indicates the rural reference we will later use to compute the UHI, which is around 70 km from downtown NYC and dominated by broadleaf deciduous vegetation. The average elevation of the rural reference is 100–150 m above sea level

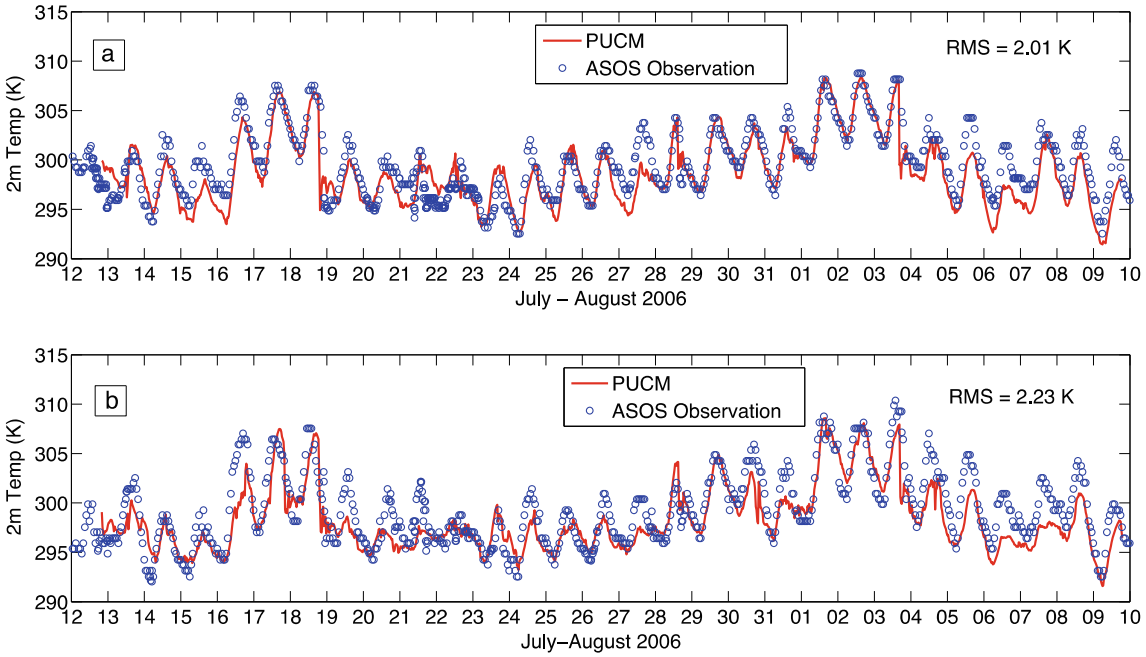

Fig. 3 Evaluating PUCM simulated 2-m air temperature against ASOS observations. Top panel (a) Central Park station, bottom panel (b) JFK Airport station

on the factors that affect UHI. Subsections 4.1 and 4.2 analyze the surface conditions during the heatwave episodes. In subsection 4.1 the UHI is used as an indicator to quantify the impact of heatwaves. Subsection 4.3 analyzes how various factors such as heat storage capacity, secondary circulation, and soil moisture deficit influence UHI.

4.1 The UHI and heatwaves

New York City experienced two major heatwave episodes during the July–August period in 2006: one between July 17th and July 19th and another between August 1st and August 3rd. The definition of a heatwave is ambiguous and

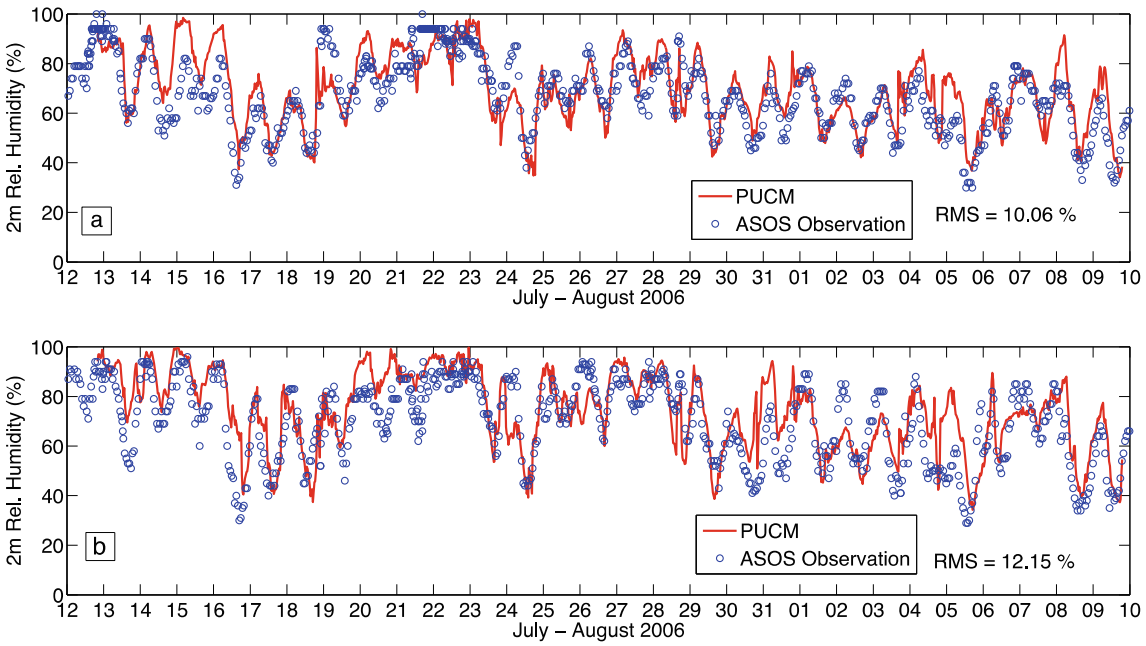

Fig. 4 Evaluating PUCM simulated 2-m air relative humidity against ASOS observation. Top panel (a) Central Park station, bottom panel (b) JFK Airport station

varies geographically. It is also closely associated with the human health impacts and heat-related illness. In this article, a heatwave is defined as an extended period (three or more days) when the daily maximum temperature exceeds 306 K (over 90 °F). During the July heatwave, most of the continental USA was under a massive high-pressure zone, leading to the formation of a sharp ridge over the NYC area. As a result, the area also experienced lower than normal wind speeds. During the August heatwave episode, a dominant surface high and an upper level ridge resulted in clear skies and warm weather over the city. In this period, between July 13th and August 9th, the average (over all days) maximum and minimum temperature in NYC was 304 K (87 °F) and 296 K (73 °F), respectively. These values were 2 K above normal, and the temperatures during the two heat wave periods were even higher as illustrated in Fig. 3. During the second heatwave episode, the La Guardia airport station recorded three consecutive days when the maximum temperature reached above 311 K (100 °F). In this total period, the total precipitation in NYC was less than 6 mm, while the normal average is around 80 mm.

To visualize the surface conditions, 2-m temperature contours and 10-m wind vectors for domain 3 are shown in Fig. 5. The series of snapshots depicts the evolution of surface conditions during the first heatwave episode from July 16th, 2006, 0400 UTC, to July 18th, 2006,1900 UTC. On July 16, before the heatwave sets in, 0400 UTC (0000 EDT, panel a), the 2-m temperature in NYC averages around 24 °C and decreases as one moves away from the center of the city. The area immediately surrounding the city averages around 22 °C; the temperature at the northwestern corner of the domain (rural reference) averages between 16 and 18 °C. During this period, the surface wind, particularly within NYC, is less than 5 m s^{-1}, indicating very calm conditions. In the highly convective mid-afternoon period, 1900 UTC (1500 EDT, panel b), the 2-m temperature in the city averages around 28–30 °C and patches of 32 °C are visible at the southern edge of Manhattan, which is the downtown area with a dense concentration of high rises. The area immediately to the west of NYC, the very densely built eastern New Jersey, also experiences elevated temperatures. It should be noted that the temperature at the rural reference (northwestern part of the domain) is also high at about 28–30 °C. While there is considerable cooling during the night (panel c), parts of NYC still remain at 28–30 °C. The wind speeds are also much lower compared to the previous night and show no large-scale pattern. On 1900 UTC (1500 local time, panel d), July 17th, the heatwave sets in and the entire NYC area experiences high and uniform temperatures of 32–34 °C. The rural reference is 2–3 °C cooler than the urban core of NYC. The wind speed averages between 5 and 10 m s^{-1} and the winds are predominantly from the west. On the night of July 18th (panel e), the temperature in NYC is still in excess of 30 °C. There is nearly a 5 °C difference between NYC and the rural reference point. The temperature contour and the wind vectors on July 18th 1900 UTC (panel f) are similar to those observed on July 17th 1900 UTC. As the heatwave episode comes to an end, the region cools down and the temperature on the night (panel g) and mid-afternoon (panel h) of July 19th is considerably lower compared to the previous day.

The area adjoining the city is highly urbanized, particularly the area to the west of NYC. Eastern New Jersey is a vast residential enclave and an important industrial center. During the heatwave period, this part of the domain experiences high temperatures and becomes a hotspot that has the potential to act as a buffer zone that reduces the advective cooling effect associated with rural-urban circulation (or when the wind is blowing from the west).

To understand the impact of the urban landcover on the near surface air temperature, the spatially averaged 2-m temperature from NYC is compared to the spatially averaged 2-m temperature from the rural reference in Fig. 6. All the grid cells within the city limit (including the Burroughs of Manhattan, Brooklyn, Queens, the Bronx, and Staten Island), excluding the water cover, were averaged to obtain the urban time series. As mentioned, the rural reference is an area about 60 km to the northwest of the city (refer to Fig. 2). Due to the extensive urban sprawl surrounding NYC, this was the nearest rural reference to NYC. The rural land cover mainly consisted of deciduous broadleaf vegetation. The rural temperature was corrected for difference in elevation using the environmental lapse rate. From the time series, distinct temperature peaks at both urban and rural areas are visible during the mid-July and early August heatwave episodes. While the spatially averaged 2-m temperatures peaked close to 28 °C in urban areas on non-heatwave days, during the heatwave episodes, the average peaks are close to 34–35 °C. The corresponding spatially averaged rural temperature exceeded 32 °C during the heatwave episodes. The difference between the urban and rural temperatures is severe during the early morning hours just before sunrise; on average, it was 2–4 °C warmer in the city compared to the surrounding rural area. It should also be noted that while the slope of urban and rural temperatures are similar during the early morning and the noon period, the rural area cools down faster compared to the urban area in the afternoon hours. This difference in cooling is mainly related to the high thermal storage in built materials as well as to anthropogenic heat releases and to urban morphology. Concrete is a particularly effective store for heat compared to the natural land cover over rural areas (Ramamurthy et al. 2014). Built materials effectively absorb incoming radiation and store the heat during the daytime, subsequently releasing it back into the atmosphere as sensible heat long after sunset.

The urban-rural contrast is illustrated in Fig. 7 more vividly. The UHI index shown in the figure was calculated as the difference between the urban and rural spatially averaged 2-m

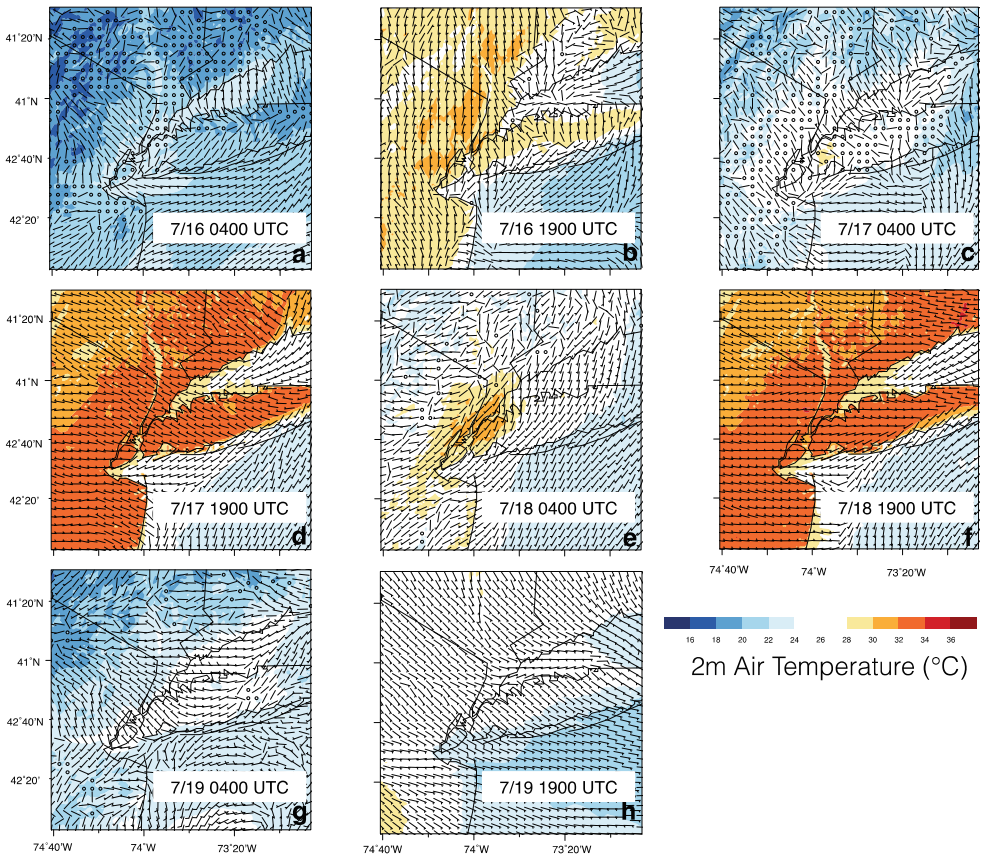

Fig. 5 Evolution of surface conditions during the first heatwave episode. 10-m wind bars overlaid on 2-m temperature colormaps

temperatures. The index was computed for each time step of the simulation, and then averaged based on the time of the day for the heatwave and non-heatwave periods separately, to obtain the average diurnal UHI cycle. On regular days, the UHI intensity is highest (3.5–3.7 °C) during the nighttime and early morning hours before sunrise. The difference between urban and rural temperatures diminishes during periods with strong solar insolation due to increased atmospheric mixing: a low of 0 °C is observed between 1200 and 1500 EDT. During the heatwave episodes, while the UHI diurnal cycle pattern is similar, there exists considerable difference in amplitude. Particularly during the mid-afternoon period (1300–1800 EDT), the UHI averages around 1–3 °C as opposed to 0–1 °C during regular days. This plot clearly illustrates how heatwaves accentuate UHI intensity in NYC. This hazardous difference could be attributed to lower wind speeds in urban areas during heatwaves, to higher heat absorption and storage capacity, or to lower moisture retention and subsequent evaporation in urban areas. The succeeding sections of this article will investigate the relative contributions of these influences.

4.2 Influence of warm/cool advection

Figure 8 compares the 850-mb height wind vectors overlaid on the temperature contours at the same level during a heatwave period and during a regular day; both snapshots

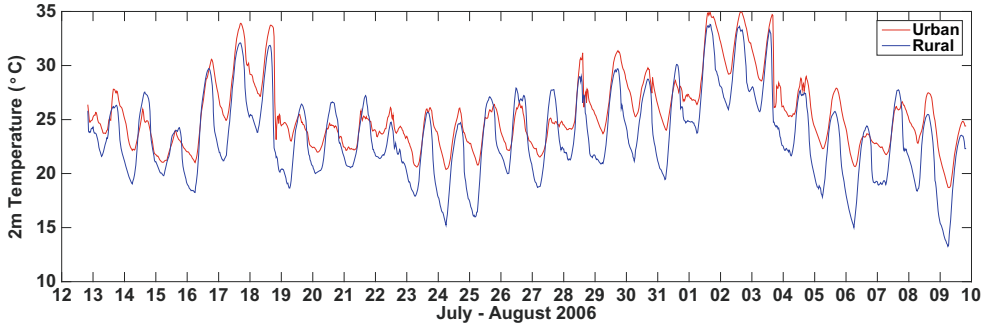

Fig. 6 Spatially averaged 2-m air temperature from NYC and from the rural reference for the entire simulation period

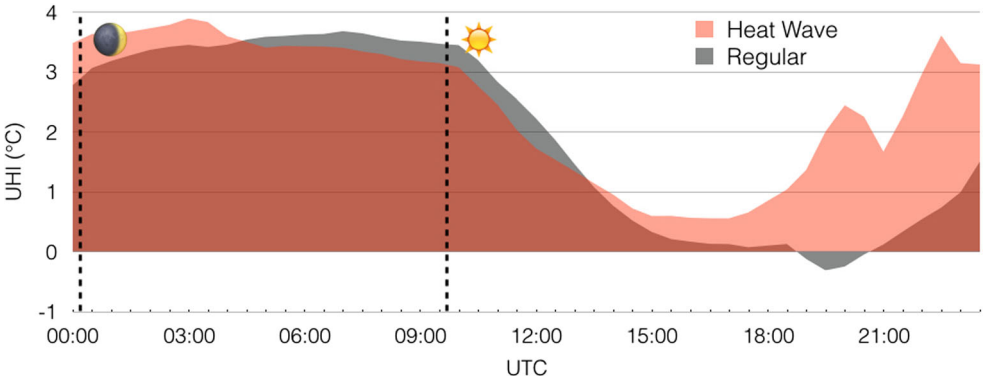

Fig. 7 Averaged diurnal cycle of the UHI for NYC for regular (21-day average) and heatwave (6-day average) days

were taken at 1400 EDT. The figure is from the 9-km resolution domain 1. On the regular day, strong southwesterly winds are visible and influence the entire mid-Atlantic and northeastern coastal areas. In the NYC region, sea winds are penetrating through the Long Island region and sweeping inland, thereby cooling the urban core of NYC. The 850-mb temperature around NYC varies between 289 and 292 K. During the heatwave period, a strong anticyclonic high-pressure region is centered in Virginia, to the southwest of Washington DC. The 850-mb temperature averages around 292–295 K over the NYC area. The wind speeds around the high-pressure area are extremely weak, averaging less than 3 m s^{-1}. Away from the eye of the anticyclone, the wind speeds increase marginally. In the NYC area, the coastal winds that normally penetrate (seen during regular days) the region are completely absent; the winds are predominantly from the west.

The southwesterly wind pattern visible in Fig. 8a was a regular feature during the normal days of the simulation period. This can be viewed in Fig. 9, which compares the 10-m wind roses for regular (a) and heatwave (b) days in domain 3 over NYC. During the regular days, winds were mainly from the south-southwest direction, accounting for nearly 60 % of the overall winds. During this period, milder winds from the north are also visible. These northerly winds were present during the nighttime period. In stark contrast, during the heatwave episodes, the winds were predominantly from the west. Winds from all other sectors were negligible. The diurnal pattern seen during the regular days is also completely absent during the heatwave. It is also important to note that in the NYC region, no noticeable change in the wind speeds are seen during the heatwave period compared to regular days, with winds between 4 and 7 m s^{-1} dominating in both periods, precluding wind speed as a major factor in the interaction between UHI and heatwaves for this episode (data from both episodes will be analyzed more thoroughly in the next section). Therefore, the change in the wind direction, which precludes cooling of NYC by southwesterly coastal winds during the heatwave, could be one of the crucial factors in elevated UHI in the city during the mid-afternoon periods of heatwave episodes.

To further investigate the role played by coastal winds, the near surface air temperature during the daytime period (0900–0500 EDT) is shown as function of distance from the coast in Fig. 10. The horizontal distance of each grid cell from the Atlantic coast was computed, and the difference between the 2-m temperature in that grid cell (T) and the 2-m temperature averaged over all grid cells (T_m) was then computed (only urban grid cells were considered for this plot). The temperature differences were then averaged for a given distance from the coast and plotted in Fig. 10. The figure shows that, for regular days, the daytime 2-m temperature is lower than the spatial average close to the coast (<5 km). The sea breezes on average penetrate 3–5 km inland. Between 5 and 12 km, the temperature remains steady and equal to the regional average, but then increases rapidly beyond that point, to become almost 0.7 °C above average. This illustrates the efficiency of coastal wind cooling during regular days. The daytime near surface air temperature on heatwave days on the other hand shows no such spatial variations with distance from the coast. T–T_m remains close to 0 for the first 20 km from the coast. The westerly winds that result from the high-pressure system block the sea breeze and advect hot air into the NYC area, keeping the air temperature relatively homogeneous over land. The cooling coastal winds are completely absent. Two other studies, Meir et al. (22) and Gedzelman et al. (2003), have also highlighted the influence of coastal wind on UHI in NYC.

4.3 Factors that influence UHI

In this section, we discuss the influence of the primary factors that modulate the UHI, namely wind speed, heat storage capacity, and soil moisture.

4.3.1 Wind speed

High wind speeds would result in stronger advective cooling. As wind speed increases, the volume of relatively cooler air brought from the surrounding rural areas, or for coastal cities like NYC from the coastal waters, becomes highly effective in

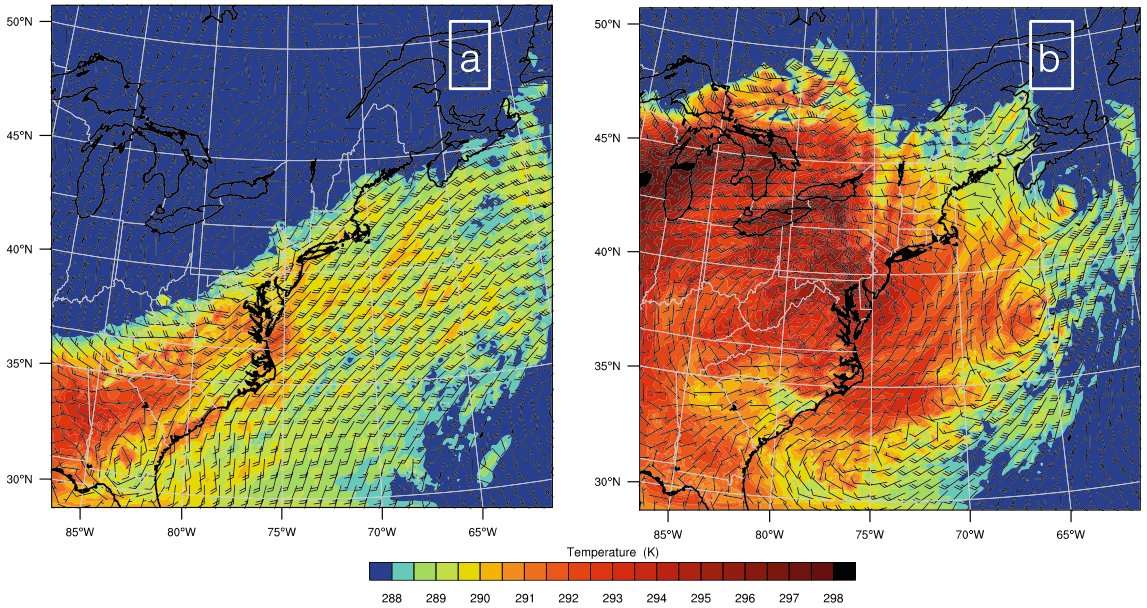

Fig. 8 A 850-mb wind and temperature difference between a regular day (**a**, July 23, 1500 EDT) and a heatwave day (**b**, July 16, 1500 EDT)

reducing the urban temperature. These winds can be the results of regional synoptic patterns (like the coastal wind cooling depicted in Fig. 10) or of smaller scale secondary circulations. Since urban areas are hotter than the surrounding environment, the thermals generated during the convective period lift the hot mass of air vertically. Urban areas also experience stronger convection due to higher turbulent heat transfer associated with stronger surface heat flux. These vertical motions create a favorable horizontal pressure gradient for the cooler air from the neighboring areas to sweep in. These secondary circulations could potentially play a crucial role in reducing the horizontal temperature gradient between urban and rural areas. However, when the simulations conducted here were analyzed, the magnitude of wind speed had very minimal impact on UHI magnitude. The correlation between wind speed and UHI (not shown here) was very weak (regression coefficient = 0.06) throughout our study period. The wind direction on the other hand does have a significant influence as illustrated in Fig. 10, which revealed the key role played by coastal winds.

4.3.2 Storage flux

Storage flux is another important factor that determines the magnitude of the temperature difference between the urban and the surrounding rural area. The equation below explains the urban surface energy balance for a volume of outdoor space, extending from the ground

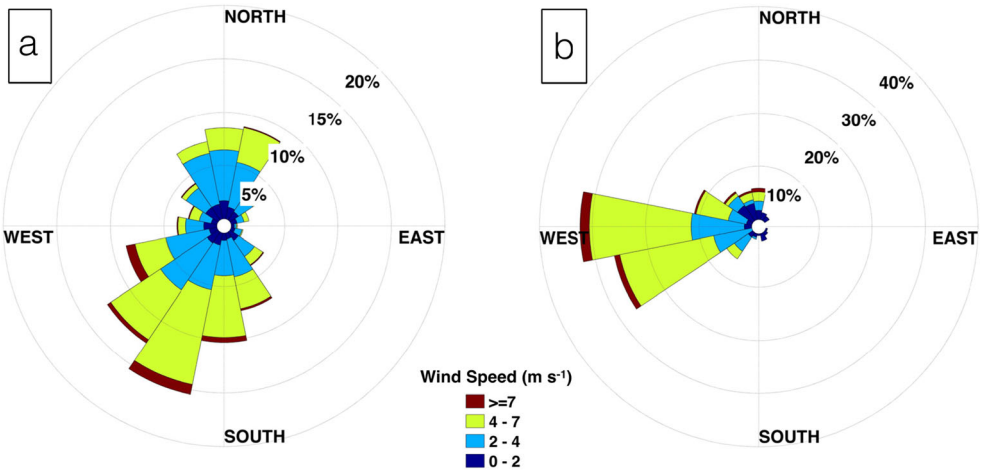

Fig. 9 Surface wind roses (10 m) for regular days (**a**) and heatwave days (**b**)

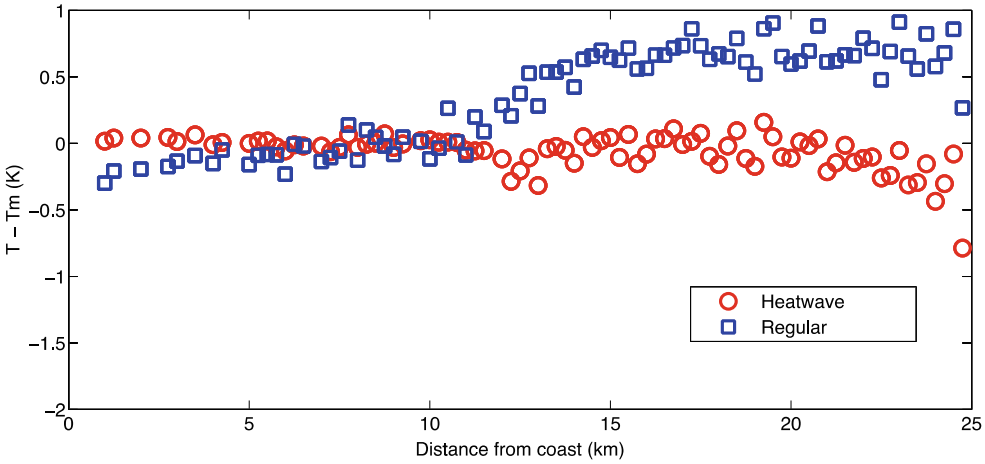

Fig. 10 Average daytime temperature difference (relative to the areal average over the same period) in NYC as a function of distance from the coast

(including an infinitesimal interfacial layer below the surface) till the top of buildings.

$$AE = R_n - G = H + \mathrm{LE} + A \quad (2)$$

R_n represents the net sum of all four radiative components (incoming and outgoing longwave and shortwave radiation). Over urban areas, all four components of radiation are disturbed from their rural balance. The built surfaces that dominate the urban areas, particularly black roofs, asphalt roads, and parking lots, decrease the overall albedo, and as a result, more energy is absorbed and the magnitude of the outgoing shortwave radiation is reduced while the magnitude of outgoing longwave radiation is increased. G represents the storage flux and is one of the most crucial terms in the urban areas. In our simulations, G is computed as the residual. While G over rural surfaces account for less than 10 % of the total energy, in urban areas, G is the most dominant term during the convective period (Ramamurthy et al. 2014). Built surfaces, particularly concrete, due to their high heat capacity, act as thermal reservoirs. This heat stored during the daytime is released as sensible heat during the nighttime periods, long after sunset. This process aids in keeping the urban surfaces as sources of heat all through the day. H and LE denote the sensible and latent heat fluxes. Over urban areas due to reduction in moisture availability, the sensible heat flux is higher compared to latent heat flux (relative to the rural vegetated surfaces). Finally, A represents the anthropogenic heat emissions; output from heat ventilation and air conditioning system (HVAC), industrial plants, and vehicle combustion can be large in urban areas. Values as high as 400 W m^{-2} have been reported over highly urbanized cities (Kanda 2007).

The scatter plot in Fig. 11 shows a linear trend between storage flux and UHI, with a steep negative slope. High UHI values are associated with high negative urban storage flux. The negative flux values indicate heat released from urban areas that occur after sunset when urban surfaces start cooling. When storage flux values are low, between 0 and −25 W m^{-2}, the UHI values range between 2 and 3 K. As storage flux increases beyond −40 W m^{-2}, UHI increases rapidly. The average UHI is around 6 K for storage flux greater than −70 W m^{-2}. In general, high UHI values are observed in the nighttime when the difference in urban and rural storage fluxes is higher. This difference mainly controls the diurnal variability in UHI. It should be noted that the simulations do not account for anthropogenic heat emissions due to uncertainty/non-availability in their estimates; however, in NYC, this term could be significant.

4.3.3 Moisture availability

The other key factor that could potentially influence UHI is moisture availability. Surface water controls the partitioning of surface fluxes into latent and sensible heat and directly influences the temperature in the atmospheric boundary layer. Previous simplified modeling of UHI development in fact suggests that this is the most important physical parameter in determining the strength of the UHI and its interaction with heatwaves (Li and Bou-Zeid 2013). Built surfaces are nearly devoid of moisture retention capacity compared to natural surfaces, and hence, urban areas profusely distribute available energy to sensible heat. Evaporation from impervious surfaces is only significant immediately following rain events (Ramamurthy and Zeid 2014). Unlike available energy and wind characteristics, moisture availability does not vary diurnally and is related to precipitation and surface and soil characteristics. While UHI intensity varies over a diurnal cycle with the surface energy budget partitioning as illustrated in the previous section, the long-term trends of daily-averaged intensity could be controlled by moisture availability. Moisture availability is also the primary factor that governs the large-scale climate dynamics in the soil-vegetation-atmosphere continuum. Previous studies have underlined the relationship between soil moisture deficit and the triggering of heatwaves (Fischer et al. 2007).

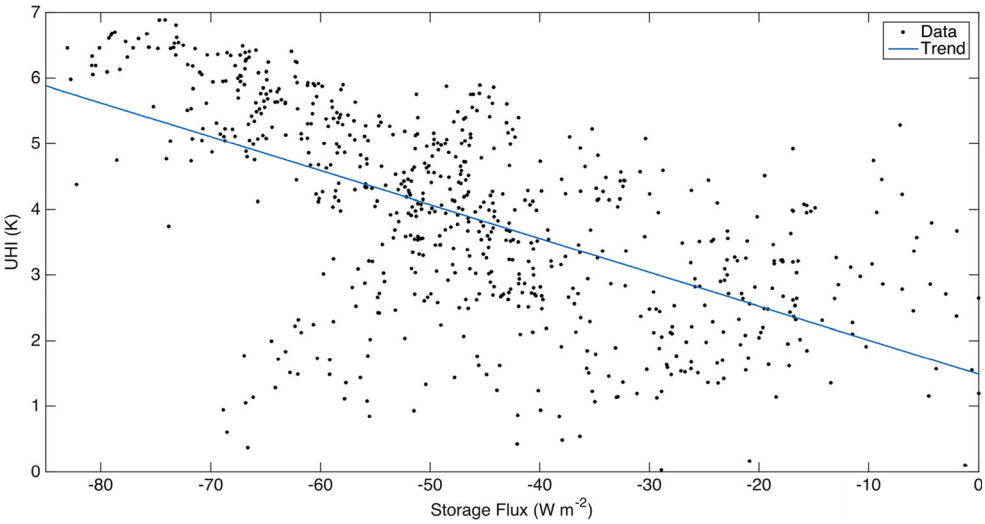

Fig. 11 Scatter plot relating storage flux in urban areas to UHI in NYC (regression coefficient = 0.72)

The area-averaged volumetric top soil moisture time series is depicted in Fig. 12. The plot shows a significant deficit in moisture availability between the urban and rural soils. The rural areas peak at 0.35 and the values never decline below 0.27. In contrast, the averaged urban volumetric top soil moisture content (taken from the mosaic version of WRF over vegetated lands only) is 0.22 and dips as low as 0.17. The wilting point for the urban soil is close to 0.12. Compared to the rural surface, the urban soils also dry and lose their wetness relatively faster. This is evident from the noticeably higher negative slope of the urban soil moisture time series. This inability to hold moisture, as seen in Fig. 12, is related to the low vegetative fraction in urban areas, which leads to an arid atmosphere that increases soil drying. It should however be noted that engineered urban soil layers can also suffer from compaction that decreases infiltration rate and increases runoff (Gregory et al. 2006), or in other cases, sandy soils with low moisture retention capacity could be used to enhance infiltration and mitigate flooding, further reducing soil moisture. However, these effects are not part of the modeling framework since urban soils are not been explicitly classified in land surface models (we simply use the USGS SSURGO data). Moreover, the unique mosaic approach adapted in our numerical simulation helps us to visualize the drying of urban soil. In the default WRF model, which classifies the grid cells based on dominant land use category, the dense urban grid cells will be mostly impervious.

Note that the volumetric soil moisture time series graph details the moisture availability of vegetated soils (urban or rural) as explained earlier and is thus not the actual area-averaged availability. The engineered built surfaces that dominate urban areas lack porosity and have an almost negligible moisture retention capacity compared to vegetated surfaces. Therefore, the net available moisture in urban terrain, per unit area, will be significantly lower when the dry impervious surfaces are accounted for. To illustrate this difference, the actual moisture availability $\sigma_f\,\theta$, here θ, represents the top surface (4 cm) volumetric soil moisture and the σ_f represents the vegetative fraction in the grid cell, averaged over the entire period is shown in Fig. 13. The moisture availability contours depict a contrasting picture. The rural background in the northwest corner averages a little over 0.3, while the urban core of NYC averages around 0.03 over the entire 28-day period. In general, there is 10 times less surface moisture available in NYC compared to the nearby rural areas. The land cover immediately surrounding NYC also lacks moisture. The eastern end of New Jersey and the Long Island area average a $\sigma_f\,\theta$ around 0.05 to 0.075. As we move farther from the city, the moisture availability gradually increases.

The deficit in the moisture availability shown above can have serious implications on thermal comfort in cities. Over rural areas, the available moisture is mostly converted to latent heat flux as opposed to sensible heat. The average mid-day (1100–1500 EDT) Bowen ratio (ratio of sensible heat to latent heat) over the rural surface is 0.44. In stark contrast, the Bowen ratio over the urban core of NYC is 13. Particularly, the period from the end of July to the first 10 days of August experienced a severe dry down period, when the urban Bowen ratio was as high as 15.5. This influence of soil moisture on surface fluxes translates into an influence on air temperature, as can be deduced from observing the strong negative spatial correlation between the soil moisture field in Fig. 13 and the temperature field in Fig. 2. A temporal correlation is however more difficult to establish due to the longer time scales over which soil moisture varies compared to the much shorter temporal variability scales of air temperature.

To assess the influence of soil moisture deficit temporal trends on the UHI, one can also compute a commonly used indicator of water availability defined as follows (Brutsaert 2005):

$$\beta = \frac{\theta - \theta_w}{\theta_w - \theta_s} \tag{3}$$

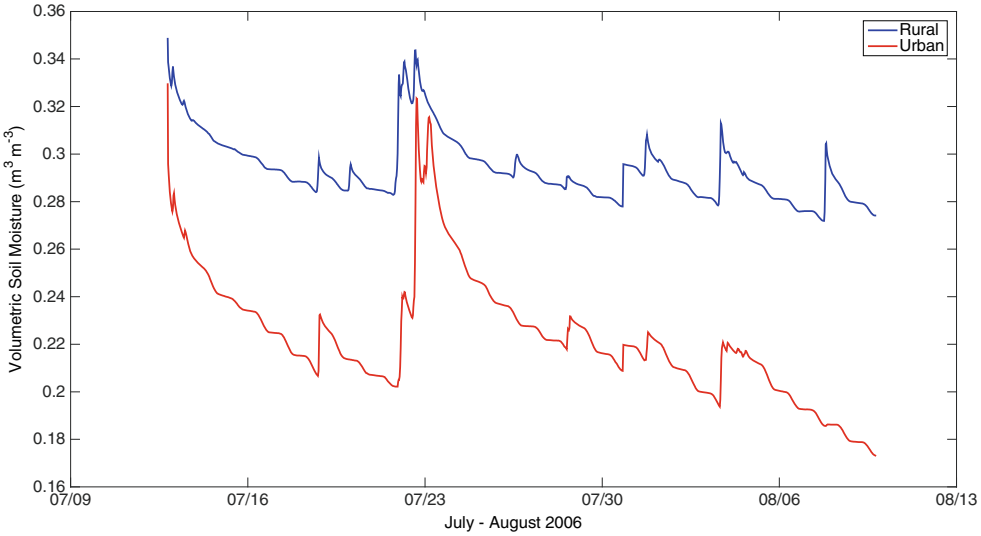

Fig. 12 Spatially averaged volumetric surface soil moisture (top 4 cm from ground level) for NYC and the rural reference

In Eq. 3, θ represents the volumetric soil moisture and θ_w and θ_s represents the wilting point and saturation point. β in the above equation is actually the reduction factor that distinguishes actual evaporation (E) from potential evaporation (E_p):

$$E = \beta E_p \tag{4}$$

Using this β, the moisture availability deficit β_D between the urban and rural areas can be calculated as

$$\beta_D = \left(1 - \frac{\beta_u}{\beta_r}\right) \tag{5}$$

In the above equation, β_u and β_r are the urban and rural reduction factors, respectively. A β_D of 0 indicates equal

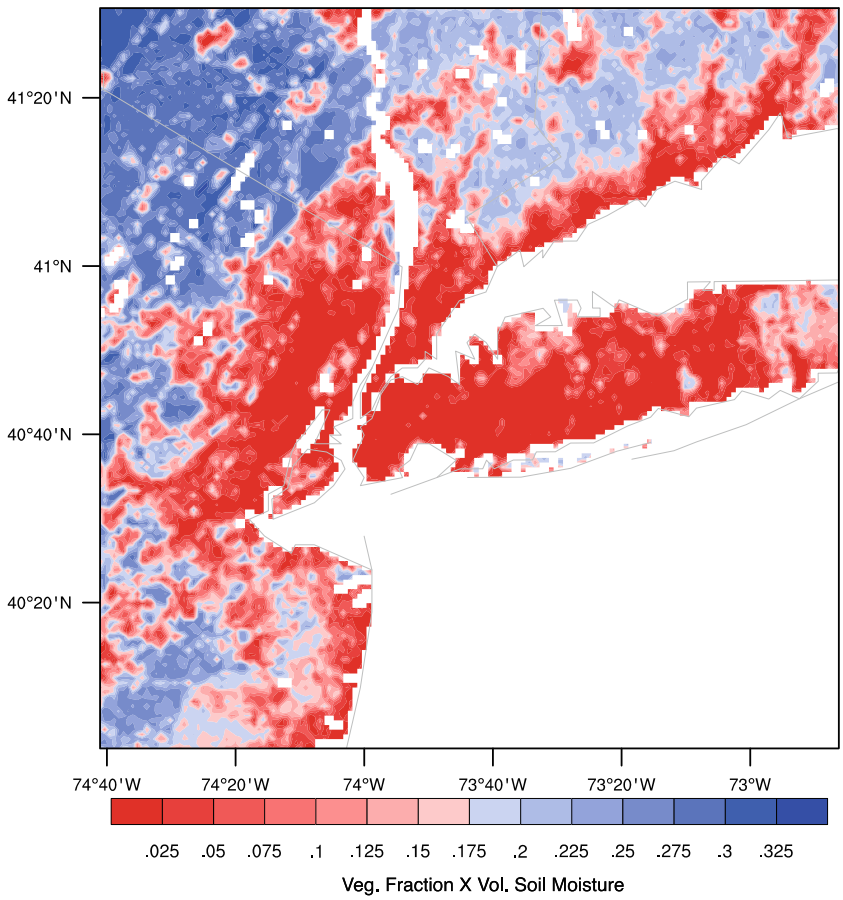

Fig. 13 Contour showing the actual moisture availability in the simulation domain (domain 3), averaged over the entire simulation period

moisture availability in urban and rural areas while a value of 1 denotes a completely dry urban surface. During the simulation period, β_D varied considerably; the average β_D was close to 0.2 and reached a low of 0.09 following a rain event on July 23rd. On heatwave days on the other hand, β_D increased to nearly 0.3. A severe dry down period persisted from July 28th till the end of the simulation period, during which the β_D peaked close to 0.4. The UHI values were significantly amplified in these dry down periods. The average nighttime UHI in NYC increased from 2.5 to 4.5 °C. These results indicate that moisture availability could play a vital role in controlling the long-term trend in UHI in NYC. During the second half of the simulation period, when NYC experienced a long dry down period, the UHI kept increasing.

Apart from the citywide influence witnessed in our simulation, the lack of soil moisture has wider implications from a regional climatology perspective. Several regional climate studies have postulated a link between extreme events like heatwaves and soil moisture deficit. In one of the well-documented and reported recent heatwave episodes (Fischer et al. 2007), unusual dry conditions, combined with circulation anomalies, lead to a 2-week long heatwave event that centered on southern France. Strong variability in soil moisture anomalies could also lead to local/mesoscale circulations that affect precipitation patterns (Seneviratne et al. 2010). These induced precipitation deficits favor hot extremes. On a global scale, the occurrence probability of an above average hot summer day preceding a precipitation deficit is as high as 60 % in North America (Mueller and Seneviratne 2012).

Currently, urban soils are poorly represented in land surface models. As discussed earlier, urban soils are severely disturbed and highly heterogeneous. But very few studies have been conducted to understand their physical and thermal characteristics. Also direct observations of urban soil moisture are rare and satellite products are too coarse and uncertain over built terrain. In order to improve our understanding of the role played by urban-rural soil moisture deficit in exacerbating the urban thermal environment and improve the representation of urban soils in land surface models, more direct observations are needed.

5 Conclusion

This study used a modified version of the WRF model to simulate two heatwave episodes. The UCM in the standard WRF model was replaced by the PUCM that has sub-facet level representation for urban fluxes and more realistic hydrology. The dominant land use categorization approach used in WRF was substituted with a mosaic approach that computes land surface fluxes for every land use type in a particular grid cell and fractionally averages them. This mosaic scheme coupled with the PUCM has vastly improved the urban representation in WRF, resulting in simulations that are consistent with remote sensing data and single-point observations.

Our analysis indicates that the heatwaves amplify the UHI in NYC, in agreement with our previous studies over smaller cities (Li and Bou-Zeid 2013). Particularly during the mid-afternoon period during heatwave episodes, the UHI increases by 1.5–2 °C. This increase would have very adverse implications on mortality and morbidity in cities (Anderson & Bell 2011).

Our results also indicate that moisture availability and storage heat flux played a crucial role in controlling the UHI in NYC, with wind speed playing a lesser role. Storage flux was shown to have a linear relationship with a 30-min averaged UHI in NYC. However, the correlation with wind speed is relatively weak, indicating it was a secondary factor. Wind direction on the other hand was a major influence on the microclimate in NYC. During the heatwave episodes, the southeasterly winds that are frequent in the afternoon periods during regular summer days were deflected by the strong westerlies, a result of the anticyclonic depression. These southwesterly winds are essential to moderating the UHI during the summer months in NYC since they result in strong advective cooling by sea breeze. The lack of coastal winds in the afternoon periods during heatwave episodes adversely affects the daytime UHI.

The results also highlight the crucial role played by moisture availability in controlling the overall strength of UHI in NYC. The difference in evaporative fraction between the urban and rural areas was shown to have a significant influence on the daily-averaged UHI. The built surfaces that dominate the urban area lack moisture retention capacity. Furthermore, the arid urban atmosphere accelerates the desiccation during dry down periods, thereby amplifying the moisture availability deficit between the urban and the surrounding rural areas. While moisture deficit has been found to play a crucial role in exacerbating extreme heat events on a regional scale, our results here further indicate that, even at the city scale, the moisture availability deficit tends to play a major role in maintaining elevated temperatures in urban areas.

Acknowledgments This work was supported by the Helen Shipley Hunt Fund through Princeton University and by the US National Science Foundation under grant CBET-1058027. The simulations were performed on the supercomputing clusters of the National Center for Atmospheric Research through project P36861020.

References

Altman P (2012) Killer summer heat: Projected death toll from rising temperatures in America due to climate change. National Resources Defense Council, Ib:12-05-C.

Anderson GB & Bell ML. 2012. Lights out. Epidemiology (Cambridge, Mas) 23(2), pp. 189–193

Black E et al. (2004) Factors contributing to the summer 2003 European heatwave. Weather 59(8):217–223

Bornstein RD (1968) Observations of the Urban Heat Island Effect in New York City. J Appl Meteorol 7(4):575–582
Brutsaert W (2005) Hydrology: an introduction. Cambridge University Press, Cambridge
Bureau UC (2011). 2010 Census, Population Division.
Chen F, Zhang Y (2009) On the coupling strength between the land surface and the atmosphere: from viewpoint of surface exchange coefficients. Geophys Res Lett 36(10):L10404
Dudhia J (1989) Numerical study of convection observed during the winter monsoon experiment using a mesoscale two-dimensional model. J Atmos Sci 46(20):3077–3107
Ellis FP, Nelson F (1978) Mortality in the elderly in a heat wave in New York City, August 1975. Environ Res 15(3):504–512
Fischer EM et al. (2007) Contribution of land-atmosphere coupling to recent European summer heat waves. Geophys Res Lett 34(6): L06707
Gaffin SR et al. (2008) Variations in New York City's urban heat island strength over time and space. Theor Appl Climatol 94(1–2):1–11
Gedzelman SD et al. (2003) Mesoscale aspects of the urban heat island around New York City. Theor Appl Climatol 75(1–2):29–42
Giannaros TM et al. (2013) Numerical study of the urban heat island over Athens (Greece) with the WRF model. Atmos Environ 73:103–111
Gregory JH et al. (2006) Effect of urban soil compaction on infiltration rate. J Soil Water Conserv 61(3):117–124
Hoffert MI et al. (2002) Advanced technology paths to global climate stability: energy for a greenhouse planet. Science 298(5595):981–987
Kanda M (2007) Progress in urban meteorology: a review. J Meteorol Soc Jpn 85(0):363–383
Klein Rosenthal J, Kinney PL, Metzger KB (2014) Intra-urban vulnerability to heat-related mortality in New York City, 1997–2006. Health & Place 30:45–60
Kusaka H et al. (2001) A simple single-layer urban canopy model for atmospheric models: comparison with multi-layer and slab models. Bound-Layer Meteorol 101(3):329–358
Leahey DM, Friend JP (1971) A model for predicting the depth of the mixing layer over an urban heat island with applications to New York City. J Appl Meteorol 10(6):1162–1173
Li D, Bou-Zeid E (2013) Synergistic interactions between urban heat islands and heat waves: the impact in cities is larger than the sum of its parts. J Appl Meteorol Climatol 52(9):2051–2064
Li D, Bou-Zeid E (2014) Quality and sensitivity of high-resolution numerical simulation of urban heat islands. Environ Res Lett 9(5): 055001
Li D et al. (2013) Development and evaluation of a mosaic approach in the WRF-Noah framework. J Geophys Res-Atmos 118(21):11,918–11,935
Li D, Bou-Zeid E, Oppenheimer M (2014) The effectiveness of cool and green roofs as urban heat island mitigation strategies. Environ Res Lett 9(5):055002
Li D et al. (2015) Contrasting responses of urban and rural surface energy budgets to heat waves explain synergies between urban heat islands and heat waves. Environ Res Lett 10(5):054009
Martiello MA, Giacchi MV (2010) Review article: high temperatures and health outcomes: a review of the literature. Scandinavian J Public Health 38(8):826–837
Meehl GA (2004) More intense, more frequent, and longer lasting heat waves in the 21st century. Science 305(5686):994–997
Meir T et al. (2013) Forecasting the New York City urban heat island and sea breeze during extreme heat events. Weather Forecast 28(6): 1460–1477
Melilo J, Richmond T, Yohe G (2014) Climate change impacts in the United States: the third national climate assessment. Global Change Research Program, U. S, 841 pp. doi:10.7930/J0Z31WJ2
Mellor GL, Yamada T (1974) A hierarchy of turbulence closure models for planetary boundary layers. J Atmos Sci 31(7):1791–1806
Mlawer EJ et al. (1997) Radiative transfer for inhomogeneous atmospheres: RRTM, a validated correlated-k model for the longwave. J Geophys Res 102(D14):16663
Mueller B, Seneviratne SI (2012) Hot days induced by precipitation deficits at the global scale. Proc Natl Acad Sci U S A 109(31):12398–12403
Oke TR (1982) The energetic basis of the urban heat island. Q J R Meteorol Soc 108(455):1–24
Palecki MA, Changnon SA, Kunkel KE (2001) The nature and impacts of the July 1999 heat wave in the midwestern United States: learning from the lessons of 1995. Bull Am Meteorol Soc 82(7):1353–1367
Price JC (1979) Assessment of the urban heat island effect through the use of satellite data. Mon Weather Rev 107(11):1554–1557
Ramamurthy P & Zeid EB (2014). Contribution of i mpervious surfaces to urban evaporation. Water Resources Research.
Ramamurthy P et al. (2014). Influence of sub-facet heterogeneity and material properties on the urban surface energy budget. Journal of Applied Meteorology and Climatology. p.140331150345000.
Robinson PJ (2001) On the definition of a heat wave. J Appl Meteorol 40(4):762–775
Rosenzweig C, Solecki W (2010) Introduction to climate change adaptation in New York City: building a risk management response. Ann N Y Acad Sci 1196:13–17
Rosenzweig C et al. (2005) Characterizing the urban heat island in current and future climates in New Jersey. Global Environ Change Part B: Environmental Hazards 6(1):51–62
Rosenzweig C et al. (2009) Mitigating New York City's heat island: integrating stakeholder perspectives and scientific evaluation. Bull Am Meteorol Soc 90(9):1297–1312
Salamanca F, Martilli A, Yagüe C (2012) A numerical study of the urban heat island over Madrid during the DESIREX (2008) campaign with WRF and an evaluation of simple mitigation strategies. Int J Climatol 32(15):2372–2386
Seneviratne SI et al. (2010) Earth-science reviews. Earth-Sci Rev 99(3–4):125–161
Skamarock WC et al. (2005). A description of the advanced research WRF version 2, National Center for Atmospheric Research.
Wang Z, Bou-Zeid E, Smith JA (2011) A spatially-analytical scheme for surface temperatures and conductive heat fluxes in urban canopy models. Bound-Layer Meteorol 138(2):171–193
Wang Z, Bou-Zeid E, Smith JA (2013) A coupled energy transport and hydrological model for urban canopies evaluated using a wireless sensor network. Q J R Meteorol Soc 139(675):1643–1657 Available at: http://DOI. doi:10.1002/qj.2032
Xoplaki E, González-Rouco JF, Luterbacher J (2003) Mediterranean summer air temperature variability and its connection to the large-scale atmospheric circulation and SSTs. Clim Dyn 20(7–8):723–739
Yang J, Wang ZH, Chen F, Miao S, Tewari M, Voogt J, Myint S (2015) Enhancing hydrologic modelling in the coupled WRF-urban modelling system. Bound-Layer Meteorol 155(1):87–109
Zhang D-L, Shou Y-X, Dickerson RR (2009) Upstream urbanization exacerbates urban heat island effects. Geophys Res Lett 36(24): L24401